Automatic Detection of High-voltage Spindles for Parkinson's Disease

V. Vigneron[1,*], T. Syed[2] and Hsin Chen[3]
[1]*Electrical Department, Université d'Evry, 91020 Evry, France*
[2]*Informatics Department, National University of Computer and Emerging Sciences, Karachi, Pakistan*
[3]*Electrical Department, National Tsing Hua University, Hsinchu, Taiwan*

Keywords: Parkinson, Animal Experiment, HVS, Eigen Decomposition, Detection, Sensor Grid.

Abstract: Parkinson's disease is a progressive neurodegenerative disorder which can be characterized by several symptoms such as tremor, slowness of movements, bradykinesia/akinesia and absence of postural reflexes ... and affects 10 million people worldwide. This paper develops a novel strategy for treating patients with PD: silence High-Voltage-Spindle that resemble the pathophysiological β-waves and contribute to the development of β-waves. Silencing HVSs is expected to delay or even prevent the development of β-waves and thus the progression of PD motor symptoms. High-voltage spindles (HVSs) are observed during waking immobility of patients. In this study, the local field potentials collected from the lesioned and control rats on multiple channels were analyzed with an online detection algorithm to identify the characteristic oscillations of HVSs from the second-order statistical properties of the signals and the detection performance is investigated to obtain the optimal choices. These results provide further motivation for the real−time implementation of the automatic HVS detection systems with improved performance for pathophysiological and therapeutic applications to the thalamocortical network dysfunctions.

1 INTRODUCTION

This paper develops a novel strategy for treating patients with Parkinson's disease (PD). Hemi-PD rats will be used as a model here. We will focus on implementing a closed-loop Deep-Brain-Stimulation (DBS) system that will delay the development of the excessive beta oscillations (called β-waves henceforth). Their are found to be associated with spatial memory impairments (Radek et al., 1994), sudden arrest of ongoing behaviour and PD and to the movement abnormalities found in PD model rats. The HVSs are different from the epileptic spike-wave discharges whose dominant frequency lies in the 30−50 Hz band (Sitnikova et al., 2009) and from normal sleep spindles in both physiology aspects and signal dynamics. Indeed HVSs (i) are synchronous spike-and-wave patterns of local field potentials (LFPs) (ii) are oscillating in the 5−13 Hz frequency band (iii) are initiated in cortex whereas the sleep spindles are prevalent in sleep states (iv) can occur frequently during passive wakefulness. More, the onset and end of HVSs episodes could occasionally vary across the cortical-basal ganglia structures and thus leads to different morphological features.

Such uniqueness of HVSs demands an appropriate spindle detection algorithm with a suitable thresholding mechanism.

Although HVSs exhibit larger amplitudes than normal LFPs, the motion artifacts of an awake rat also induce large transients in LFPs. In addition, LFPs are non-stationary and coupled with non-negligible noise. These properties make it difficult to detect HVSs by simple threshold or envelope detection. Moreover, although the prominent frequency components of HVSs are around 5−13Hz, the duration of each HVS episode is only 1−4 s. Such a short duration makes it challenging to detect HVS episode at the onset by conventional frequency analysis (e.g. the *Fast-Fourier Transform*), which suffers from the trade-off between time and frequency resolutions. Based on our pilot studies, time-frequency (TF) analysis preserving the energy distribution over both time and frequency spaces is useful to extract the distinctive features of HVSs, see *e.g.* (Perumal and Chen, 2014)

*Corresponding author.
This project was funded by a PhD grant from université d'Évry number 4552013 and PHC ORCHID. The authors express their sincere thanks to the French embassy collaborators for their interest and kind permission to publish.

Vigneron V., Syed T. and Chen H..
Automatic Detection of High-voltage Spindles for Parkinson's Disease.
DOI: 10.5220/0005328503720378
In *Proceedings of the International Conference on Bio-inspired Systems and Signal Processing* (MPBS-2015), pages 372-378
ISBN: 978-989-758-069-7

who use a continuous wavelet transform (CWT) to detect the characteristic oscillations of HVSs. But the detection performance are related to a suitable choice of the wavelet parameters and the thresholding mechanism that are critical to determine the detection performance. Therefore, we will compare the features extracted by TF analysis and our proposed algorithm for detecting the distinctive features of HVSs automatically and reliably.

Finally, as this algorithm is based mainly on second-order statistics the proposed algorithm can be extended further to the FPGA-based real time systems for pathophysiological and therapeutic applications.

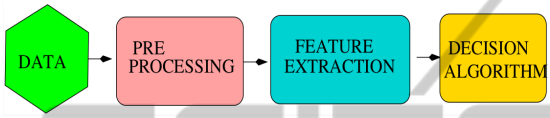

Figure 1: An overview of the HVSs detection process.

A simplified scheme in Fig. 1 gives an overview of the work.

2 DATA ACQUISITION

The PD rat models were induced in 3-4 months old Sprague-Dawley rats by unilateral injection (coordinates: AP -4.4 mm, ML +1.2 mm, V -7.8 mm relatively to bregma) of 6-OHDA in the medial forebrain bundle (MFB) at the rate of μl/min using an integrated electrophysiology instrument suitable for deep brain stimulation (DBS) procedure. Four weeks following the unilateral injection of 6-OHDA, the lesioned group of rats were determined as successful PD models through amphetamine-induced rotational behaviour (Amp, 3mg/kg, ip) by measuring the rotational speed of the lesioned rats as 6 turns per minute. The rats were unilaterally implanted bipolar stimulation electrode into the ipsilateral STN with their initial coordinates at AP -3.6 mm and L +2.5 mm. The electrode was lowered slowly along the dorsal ventral axis of brain and then advanced ventrally to the STN to obtain the electrophysiological signal with a strikingly silent structure. The EEG recordings were collected from a group of 34 lesioned rats and 20 control rats. The LFPs of the lesioned rats were recorded in both sleeping and waking immobile states in order to study the behaviour of spindling and non-spindling characteristics. The EEG patterns without artifacts and with the duration of sixty seconds were considered in the following sections to evaluate the performance of the spindle detection algorithm (see Fig. 2).

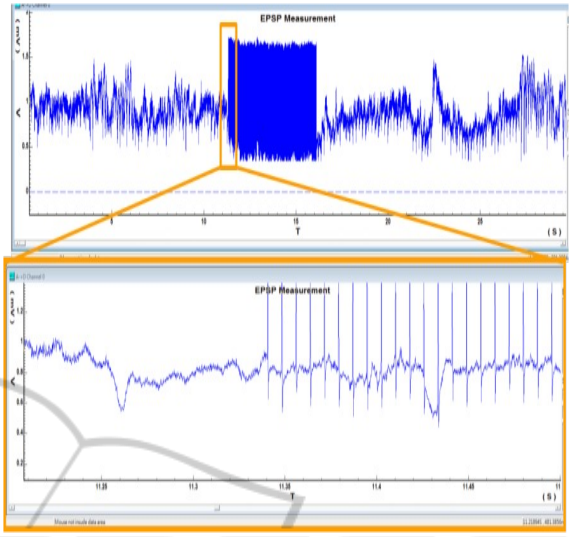

Figure 2: The LFP recorded by the micro-system during electrical stimulation (130Hz, 100 μA). The lower panel is the magnified view of the region shown in the top trace during the period when stimulation is just turned on.

3 ELIMINATION OF THE BACKGROUND NOISE

The raw artifact-free EEG recordings from lesioned (PD) and control rats (CR) are used as direct inputs to the HVS detection algorithm with a noise cancellation stage.

In the case of HVSs, there are several different causes for the noise. We can mention the defects in the sensors, the environment in which the recording is done or also the decay of the recording medium. Among all the type of noises encountered in practice, the following 2 types occur in practice:

- the background noise which can be represented by a stationary process, often originated from the electronic circuits of the amplification devices.
- the impulse noise represented as a sequence of very brief impulses, with random amplitudes and locations.

To reduce these noises and restore the signal as best as possible, we are considering them and deal with them separately. The elimination of background noise is a particular difficult problem since we have to find what characterizes the difference between the useful part of the signal and the unwanted part. We can mention (DeFreitas et al., 2012; Miyano et al., 1980; Clancy and Farry, 2000) among the different denoising methods in a stationary background noise for which the methods gives satisfactory results. They usually require for the spectral properties of the noise to be

known. They can do this by using a portion of the signal that contains nothing but noise. This portion is selected either by a direct observation of the signal or by automatically detecting the active areas of the useful signal.

We suggest here a simple *spectral substraction* leading to an acceptable result that we implemented. If we assume that the noise is white with a power σ^2 estimated from a portion of the signal containing nothing but noise, the short term amplitude spectrum of the denoised signal σ^2 is estimated by the expression:

$$\hat{X}(k) = G(k)X(k) \tag{1}$$

where

$$X(k) = \sum_{n=0}^{N-1} x(n)e^{-2j\pi nk/N}, \tag{2}$$

refers to the Discrete Fourier Transform of a length N window of the noisy signal $x(n)$ and where

$$G(k) = \begin{cases} \left(1 - \lambda \frac{\sigma\sqrt{N}}{|X(k)|}\right) & \text{if } \lambda \frac{\sigma\sqrt{N}}{|X(k)|} < 1 \\ \mu & \text{otherwise.} \end{cases} \tag{3}$$

where the parameters λ and μ are adjusted experimentally so as to obtain the best result. The results show that the background noise is rather well eliminated but the method introduces HF noises that get louder as μ decreases. In particular, $\mu = 0$ leads to the plain and simple elimination of the spectral components below the threshold, causing certain components of the noise to behave as isolated "peaks". HF noise can be reduced by decreasing λ and increasing μ but at the cost of a lower noise reduction.

The figure 3 shows the effect of the frequency domain denoising operation. λ and μ have been adjusted experimentally so as to archive the best result. This method can effectively be applied to processes that do have to be conducted in real-time. Detecting a "silent" segment automatically is not an easy task, not to say impossible to solve.

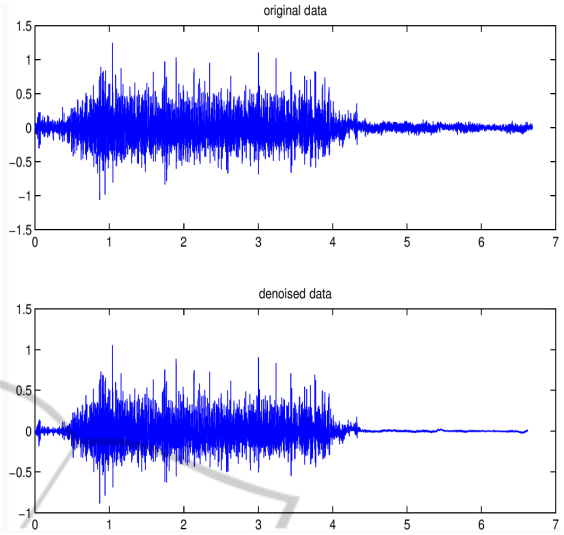

(a) Signals before and after the denoising operation

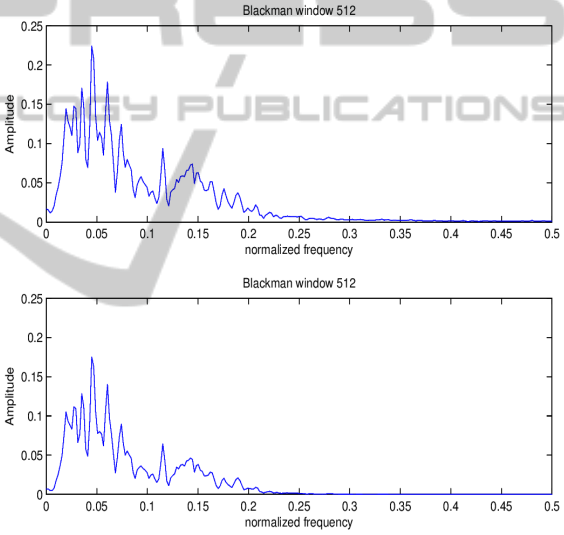

(b) Spectra of the corresponding signals

Figure 3: Noise removal demo. The frequency is expressed in normalized frequency.

4 ALGORITHMS

Collaborative signal and information processing over a network is a new area of research and is related to distributed information fusion. Processing data from many sensors generally results in better performance *e.g.* in distributed robotics (Denzler and Brown, 2002), environment monitoring, medical assistance (Vrins et al., 2004; Vigneron and Jutten, 2004), etc. but it also requires more communication resources (and thus, more energy); the reasons for this are that (i) 2 sensors don't record exactly the same signal, (ii) all sources must be involved in the recording with a non-zero variance, (iii) electrodes providing irrelevant signals can be rejected, (vi) the low power of the signal of interest can be improved, (v) there doesn't exist an optimal location of the sensors, constant in time as the "*target*" moves. These considerations in mind, in addition to the low power of the signal, may explain why the locations of the electrodes can improve the signal extraction, while others can decrease its efficiency. Therefore, one needs to consider the trade-offs between performance and resource utilization in using networked sensors. Numerous articles have dealt with this topic, but usually in the area of digital communications (Yao et al., 1998).

4.1 The Karhunen-loeve Expansion for Random Processes

We consider the situation in which n sensors are randomly distributed in a spatial region, which is 3 dimensional (the cortex) but could be less. The sensors relative positions are unknown. The sources may be narrow-band or broadband and they may be in the far or near field with respect to the sensor array. The sources do not have specific characteristics that can be used to our advantages. Due to these limitations, our initial goal is limited to the *detection*. We assume the existence of n source signals $\{s_i(t), 1 \leq i \leq q\}$ (with $n < q$), statistically independent and zero-mean and the observation of *at most* as many mixtures $\{x_i(t), 1 \leq i \leq n\}$, formed by (supposedly) linear combinations of the unknown sources, *i.e.*

$$x_i(t) = \sum_{j=1}^{q} a_{ij} s_j(t) + n_i(t), \tag{4}$$

for each $i = 1, \ldots, n$. This is compactly represented by the mixing equation $\mathbf{x}(t) = A\mathbf{s}(t)$, where the matrix $A_{(n \times q)}$ collects the mixing coefficients, $\mathbf{s}(t) = (s_1(t), \ldots, s_n(t))^T$ is a column vector collecting the *unobserved* source signals*, $\mathbf{x}(t)$ collects the n observed signals. $n_i(t)$ is a spatially white noise with zero mean and variance σ^2. Denote the $n \times 1$ sensor data vector by

$$\mathbf{x}_t = (x_1(t), \ldots, x_i(t), \ldots, x_n(t))^T.$$

$\mathbf{x}_t$ denotes a random process.

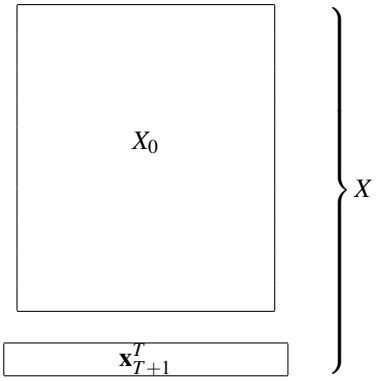

Figure 4: Augmented table.

Let X_0 be the table collecting the samples $\mathbf{x}_t, t = 1, \ldots, T$ (see figure 4) and C_0 be the covariance matrix of $\mathbf{x}$ estimated by $\hat{C}_0 = \frac{1}{T}\sum_{t=1}^{T} \mathbf{x}_t \mathbf{x}_t^T$, $\hat{\boldsymbol{\phi}}_i$ and $\hat{\lambda}_i, i = 1, \ldots, n$ the *eigenvectors* and *eigenvalues* of $\hat{C}_0$. Note that $\hat{\lambda}_i$ and $\hat{\boldsymbol{\phi}}_i$ are *estimates* of λ_i and $\boldsymbol{\phi}_i$, and that they are resp. random variables and vectors. In section 4.2, we shall show approximate formulas for the expected values and variances of these estimates. The array covariance matrix $C = E[\mathbf{x}(t)\mathbf{x}^T(t)] = ASA^T + \sigma^2 I_n$, where $S = E[\mathbf{s}(t)\mathbf{s}^T(t)]$, I_n is the $n \times n$ identity matrix. Consistent estimates of eigenvectors and eigenvalues of C are given by the eigen decomposition of the sample covariance matrix (Cover and Thomas, 1991)

$$\hat{C} = \frac{1}{T}\sum_{i=t}^{T+1} \mathbf{x}_t \boldsymbol{x}_t^T = \hat{U}_S \hat{\Lambda}_S \hat{U}_S^T + \hat{U}_N \hat{\Lambda}_N \hat{U}_N^T, \tag{5}$$

where the $\hat{q} \times \hat{q}$ and $(n-\hat{q}) \times (n-\hat{q})$ diagonal matrices $\hat{\Lambda}_S$ and $\hat{\Lambda}_N$ contain the $\hat{q}$ and $n-\hat{q}$ signal and noise subspace eigenvalues respectively. The columns of the $n \times q$ and $n \times (n-\hat{q})$ matrices $\hat{U}_S$ and $\hat{U}_N$ contain the signal and noise subspace eigenvectors, and $\hat{q}$ is any consistent estimate of q.

We wish to obtain a first-order approximation of the eigenvectors and eigenvalues of C in terms of the $\boldsymbol{\phi}_i$'s and λ_i's, where $C = C_0 + \Delta C$. Suppose that X is augmented by a bloc of values x_{T+1} (see figure 4), then

$$\hat{C} = X^T X = \begin{bmatrix} X_0^T & \mathbf{x}_{T+1}^T \end{bmatrix} \begin{bmatrix} X_0 \\ \mathbf{x}_{T+1} \end{bmatrix} = \hat{C}_0 + \mathbf{x}_{T+1}^T \mathbf{x}_{T+1} \tag{6}$$

where $\Delta C = \mathbf{x}_{T+1}^T \mathbf{x}_{T+1}$ can be seen as a (real symmetric) *perturbation* matrix. Suppose that the λ_i's are distinct. These may be obtained by retaining the terms of first order of the equation:

$$(C_0 + \Delta C)(\boldsymbol{\phi}_i + \Delta\boldsymbol{\phi}_i) = (\lambda_i + \Delta\lambda_i)(\boldsymbol{\phi}_i + \Delta\boldsymbol{\phi}_i), \tag{7}$$

where $C_0 \boldsymbol{\phi}_i = \lambda_i \boldsymbol{\phi}_i$. The resulting equation is:

$$C_0 \Delta\boldsymbol{\phi}_i + \Delta C \boldsymbol{\phi}_i \approxeq \lambda_i \Delta\boldsymbol{\phi}_i + \Delta\lambda_i \boldsymbol{\phi}_i. \tag{8}$$

To calculate $\Delta\lambda_i$, we premultiply (8) by $\boldsymbol{\phi}_i^T$ and, since $\boldsymbol{\phi}_i^T C_0 = \lambda_i \boldsymbol{\phi}_i^T$, we have:

$$\Delta\lambda_i \approxeq \boldsymbol{\phi}_i^T \Delta C \boldsymbol{\phi}_i. \tag{9}$$

The $\{\boldsymbol{\phi}_1, \ldots, \boldsymbol{\phi}_n\}$ form a complete set of basis vectors *i.e.* $\boldsymbol{\phi}_i^T \phi_j = \delta_{ij}, \forall i, j$, where δ_{ij} is the Kronecker operator ($\delta_{ij} = 1$ iff $i = j$). Hence $\Delta\boldsymbol{\phi}_i$ can be expanded as a linear combination of the $\boldsymbol{\phi}_j$'s as follows

$$\Delta\boldsymbol{\phi}_i = \sum_{j=1}^{n} b_{ij} \boldsymbol{\phi}_j, \tag{10}$$

where $\mathbf{b}_i$ are vectors of unknown parameters. From (10), $b_{ij} = \boldsymbol{\phi}_j{}^T \Delta\boldsymbol{\phi}_i$.

If we premultiply (8) by $\boldsymbol{\phi}_j^T$ and rearrange, we have for $i \neq j$:

$$b_{ij} \approxeq \frac{\phi_j^T \Delta C \boldsymbol{\phi}_i}{\lambda_j - \lambda_i} \quad (i \neq j) \tag{11}$$

To determine b_{ii}, we impose a first-order normalization condition on $\boldsymbol{\phi}_i + \Delta\boldsymbol{\phi}_i$, that is, we require

$$\|\boldsymbol{\phi}_i + \Delta\boldsymbol{\phi}_i\|^2 \approx \|\boldsymbol{\phi}_i\|^2 + 2\boldsymbol{\phi}_i^T \Delta\boldsymbol{\phi}_i, \tag{12}$$

*^{T} denotes usually the transpose operator.

and it follows that ${\boldsymbol{\phi}_i}^T \Delta\boldsymbol{\phi}_i = b_{ii} \approx 0$.
Noting that $\boldsymbol{\phi}_i^T C_0 \boldsymbol{\phi}_i = \lambda_i$ and $\boldsymbol{\phi}_i^T C_0 \boldsymbol{\phi}_j = 0$ for $i \neq j$, we summarize this section as follows:

$$\lambda_i + \Delta\lambda_i \cong \boldsymbol{\phi}_i^T C \boldsymbol{\phi}_i \tag{13}$$

$$b_{ij} \cong \begin{cases} \dfrac{\boldsymbol{\phi}_i^T C \boldsymbol{\phi}_j}{\lambda_i - \lambda_j}, & \text{for} \quad i \neq j, \\ 0, & \text{for} \quad i = j. \end{cases} \tag{14}$$

Notice that most of the approach is implicitly based on a model where the sequence $\mathbf{x}_t$ is i.i.d., *i.e.* nothing is assumed concerning temporal evolution. The algorithm detailed in (13) and (14) examine the *non-stationary case*, *i.e.* falling the 'id' in i.i.d.

4.2 Estimation of Eigenvalues and Eigenvectors

Our next task is to estimate the eigenvalues and eigenvectors λ_i and $\boldsymbol{\phi}_i (i = 1, \ldots, n)$ of the autocorrelation matrix C. For this, we calculate the sample autocorrelation matrix $\hat{C} = \frac{1}{T}\sum_{t=1}^{T} \mathbf{x}_t \mathbf{x}_t^T$ and calculate the eigenvalues and eigenvectors $\hat{\lambda}_i$ and $\hat{\phi}_i$ of $\hat{C}$. We can determine a value of T such that the estimates are sufficiently accurate. Since $\hat{C} \cong C$ for T sufficiently large, we may use the approximations (13) and (14) to express $\hat{\lambda}_i$ and $\hat{\boldsymbol{\phi}}_i (i = 1, \ldots, n)$:

$$\hat{\lambda}_i \cong \quad \boldsymbol{\phi}_i^T \hat{C} \boldsymbol{\phi}_i \tag{15}$$

$$\hat{\boldsymbol{\phi}}_i \cong \quad \boldsymbol{\phi}_i + \sum_{\substack{j=1 \\ j \neq i}} \frac{\boldsymbol{\phi}_j^T \hat{C} \boldsymbol{\phi}_i}{\lambda_i - \dot{\lambda}_j} \boldsymbol{\phi}_j. \tag{16}$$

Consider the expected value of the estimate: since the expected value of $\hat{C}$ $E[\hat{C}] = C$, therefore $E[\boldsymbol{\phi}_j^T \hat{C} \boldsymbol{\phi}_i] = \boldsymbol{\phi}_i^T E[\hat{C}] \boldsymbol{\phi}_j = \boldsymbol{\phi}_i^T C \boldsymbol{\phi}_j = \lambda_i \delta_{ij}$. It follows from (15) and (16) that

$$E[\hat{\boldsymbol{\phi}}_i] \cong \boldsymbol{\phi}_i, \quad E[\hat{\lambda}_i] = \lambda_i. \tag{17}$$

The estimates are unbiased only when the first order approximation are used, *i.e.* the bias come usually from the *second order term* of the approximation (Cover and Thomas, 1991) and the the variance comes from the first order, thus

$$E[\hat{\boldsymbol{\phi}}_i] \cong \boldsymbol{\phi}_i + \frac{1}{T} f_i, \quad E[\hat{\lambda}_i] = \lambda_i + \frac{1}{T} g_i \tag{18}$$

where f_i and g_i are functions of C, with a functional form too complex to determine.
The variances can be obtained from the first order approximation and their approximated values may be computed as follows:

$$\mathrm{var}(\hat{\lambda}_i) = E[(\hat{\lambda}_i - \lambda_i)^2] = E[\hat{\lambda}_i^2] - \lambda_i^2 \cong E[\boldsymbol{\phi}_i^T \hat{C} \boldsymbol{\phi}_i] - \lambda_i^2 \tag{19}$$

and

$$\begin{aligned} \mathrm{cov}(\hat{\boldsymbol{\phi}}_i) &= E[(\hat{\boldsymbol{\phi}}_i - \boldsymbol{\phi}_i)(\hat{\boldsymbol{\phi}}_i - \boldsymbol{\phi}_i)^T] \\ &\cong \sum_{\substack{j=1 \\ j \neq i}}^{n} \sum_{\substack{k=1 \\ k \neq i}}^{n} \frac{E[\boldsymbol{\phi}_i^T \hat{C} \boldsymbol{\phi}_j \boldsymbol{\phi}_i^T \hat{C} \boldsymbol{\phi}_k]}{(\lambda_i - \lambda_j)(\lambda_i - \dot{\lambda}_k)} \boldsymbol{\phi}_j \boldsymbol{\phi}_k^T \qquad (20) \\ &\cong \sum_{\substack{k=1 \\ k \neq i}}^{n} \frac{E[(\boldsymbol{\phi}_i^T \hat{C} \boldsymbol{\phi}_j)^2]}{(\lambda_i - \lambda_j)^2} \qquad (21) \end{aligned}$$

Note that both equations (19) and (21) are expressed as function of $E[(\boldsymbol{\phi}_i^T \hat{C} \boldsymbol{\phi}_j)^2]$.
Suppose now that the X is normally distributed, $E[(\boldsymbol{\phi}_i^T \hat{C} \boldsymbol{\phi}_j)^2]$ can be computed as follows. Let

$$\boldsymbol{\phi}_i^T \hat{C} \boldsymbol{\phi}_j = \frac{1}{T} \sum_{k=1}^{N} y_{ik} y_{jk} \quad \text{where} \quad y_{ik} = \boldsymbol{\phi}_i^T \mathbf{x}_k \tag{22}$$

and

$$\begin{aligned} E[(\boldsymbol{\phi}_i^T \hat{C} \boldsymbol{\phi}_j)^2] &= \frac{1}{T^2} \sum_{k=1}^{T} \sum_{\ell=1}^{T} E[y_{ik} y_{jk} y_{i\ell} y_{j\ell}] \qquad (23) \\ &\cong \frac{T-1}{T} \lambda_i^2 \delta_{ij} + \frac{1}{T} E[(\mathbf{y}_i^T \mathbf{y}_j)^2]. \qquad (24) \end{aligned}$$

The second subscript on $\mathbf{y}$ is dropped since the $\mathbf{x}_t$'s are identically distributed. When X is normally distributed with zero mean, the $\mathbf{y}_i$'s are also normal with $E[\mathbf{y}_i] = 0$. Therefore

$$E[\mathbf{y}_i^2 \mathbf{y}_j^2] = \begin{cases} 3\lambda_i^2 & \text{for } i = j \\ \lambda_i \lambda_j & \text{for } i \neq j \end{cases}. \tag{25}$$

Finally

$$E[(\boldsymbol{\phi}_i^T \hat{C} \boldsymbol{\phi}_j)^2] = \lambda_i^2 \delta_{ij} + \frac{1}{T}(\lambda_i^2 \delta_{ij} + \lambda_i \lambda_j). \tag{26}$$

and $\mathrm{var}(\hat{\lambda}_i) \approx \frac{2}{T}\lambda_i^2$ and $\mathrm{cov}(\hat{\boldsymbol{\phi}}_i) \approx \frac{1}{T}\sum_{\substack{\ell=1 \\ j \neq i}}^{T} \frac{\lambda_i \lambda_j}{(\lambda_i - \lambda_j)^2}$.

4.3 HVSs Detection

The HVS detection problem can be modeled as an *hypothesis testing* problem (Vigneron et al., 2010) and formulated into a maximum likelihood test we describe in the following (Johnson et al., 2011).
The observations provided by the sample process are supposed independent. The input to the detector is denoted by $\mathbf{z} = (z_1, \ldots, z_n)^T$ where z_i, $(1 \leq i \leq n)$ will consist of either noise alone, $z_i = v_i$ either signal plus noise $z_i = \hat{\lambda}_i + v_i$ computed with (15). The noise alone possibility is called the null hypothesis and is denoted by H_0. The signal plus noise possibility is called the alternative and is denoted by H_1. The detection problem may be written as testing H_0 versus H_1:

$$\begin{cases} H_0 : & z_i \sim N(0, \sigma_i^2 = \sigma_0^2) \\ H_1 : & z_i \sim N(\hat{\lambda}_i, \sigma_i^2 = \sigma_0^2) \end{cases}, \quad (i = 1, \ldots, n) \tag{27}$$

Two assumptions are made on the noise probability distributions (i) the noise components are independent, (ii) their distributions are Gaussian. The independence assumption is solely a practical requirement for the purpose of solving the equations involved. The gaussianity assumption comes from signal-space analysis of considering n-dimensional space. The choice of the Gaussian probability density function (pdf) is more interesting when computing the likelihood ratio and lead to interesting graphical interpretation. The conditional probability density of the observations $p(\mathbf{z}|H_0)$ and $p(\mathbf{z}|H_1)$ are unknown. Hence we shall rewrite the conditional density as $p(\mathbf{z}|H_k,\theta_k)$, where θ_k is a vector of unknown parameter values for which the we have no prior on the pdf and which are selected from a set Ω_k. We shall select θ_k so as to maximize $p(\mathbf{z}|H_k,\theta_k)$. Then our likelihood ratio test takes the following form:

$$\Lambda(\mathbf{z}) = \frac{\max\limits_{\theta_1\in\Omega_1} p(\mathbf{z}|H_1,\theta_1)}{\max\limits_{\theta_0\in\Omega_0} p(\mathbf{z}|H_0,\theta_0)} \underset{d_2}{\overset{d_1}{\lessgtr}} \eta. \tag{28}$$

Suppose that we take a set of n independent identically distributed observations of the preceding form. Then we must select $\theta_1 = (\mathbf{s};\Sigma)$ which maximizes the joint distribution

$$p(\{\mathbf{z}_i\}|H_1,\theta_1) = \prod_{i=1}^{T} p(\mathbf{z}_i|H_1,\theta_1) \tag{29}$$

$$= (2\pi)^{-nT/2}|\Sigma|^{-n/2}\exp\left[-\frac{n}{2}\mathrm{tr}\Sigma^{-1}S\right], \tag{30}$$

where $\Sigma = \mathrm{diag}(\mathrm{var}(\hat{\lambda}_i))$ computed with (15) and (16) is the covariance matrix of $\mathbf{z}$, S is the scatter matrix $S = \frac{1}{n}\sum_{i=1}^{n}(\mathbf{z}_i-\mathbf{s})(\mathbf{z}_i-\mathbf{s})^T$. The value of θ_1 which maximizes $p(\mathbf{z}|H_1,\theta_1)$ is $\mathbf{s} = \sum_{i=1}^{n}\mathbf{z}_i^2/n$.
We suppose that the noise variance estimate is the same for both hypothesis. Substituting these values back into the conditional probabilities of the likelihood ratio in Eq. (28) yields

$$\frac{(2\pi)^{-nT/2}|\Sigma|^{-n/2}\exp\left[-\frac{n}{2}\mathrm{tr}\Sigma^{-1}S\right]}{(2\pi)^{-Tp/2}|S|^{-n/2}\exp\left[-\frac{1}{2}\mathbf{z}^T S^{-1}\mathbf{z}\right]} \underset{d_2}{\overset{d_1}{\lessgtr}} \eta \tag{31}$$

Taking the logarithm of both side and recombining yields

$$\ell(\mathbf{z}) = \mathbf{z}^T S^{-1}\mathbf{z} \underset{d_2}{\overset{d_1}{\lessgtr}} 2\ln\eta + n(\log|\Sigma| + \mathrm{tr}\Sigma^{-1}S - |S|). \tag{32}$$

The statistic that has been identified as $\ell(\mathbf{z})$ is obviously a sufficient statistic for this problem: it will tell in which decision region $\mathbf{z}$ lies. We need the means and the variance of $\ell(\mathbf{z})$ to find the densities $p(\ell|H_0)$ and $p(\ell|H_1)$. $\mathbf{z}^T S^{-1}\mathbf{z}$ is a stochastic quadratic form. If we assume that all coordinates n_i are independent, have the same central moments σ^2, μ_4 and denote $\mathbf{a} = \mathrm{diag}(S^{-1})$, then

$$E[\ell(\mathbf{z})|H_1] = n + \mathbf{s}^T S^{-1}\mathbf{s}$$

$$\mathrm{var}[\ell(\mathbf{z})|H_1] = 2\sigma^2\mathrm{tr}(S^{-1}) + (\mu_4 - 3\sigma^2)\mathbf{a}^T\mathbf{a} + 4\mathbf{s}^T S^{-1}\mathbf{s}.$$

and

$$E[\ell(\mathbf{z})|H_0] = E[\mathbf{n}^T S^{-1}\mathbf{n}] = \mathrm{tr}(S^{-1}\Sigma) = n$$
$$\mathrm{var}[\ell(\mathbf{z})|H_0] = \mathrm{var}(\mathbf{n}^T S^{-1}\mathbf{n}) = 2\sigma^2\mathrm{tr}(S^{-1}) + (\mu_4 - 3\sigma^2)\mathbf{a}^T\mathbf{a}$$

The probability density $p(\ell|H_0)$ is therefore given by:

$$p(\ell|H_0) = K\exp\left(-\frac{1}{2}\frac{(\ell-n)^2}{2\sigma^2\mathrm{tr}(S^{-1}) + (\mu_4 - 3\sigma^2)\mathbf{a}^T\mathbf{a}}\right) \tag{33}$$

so that $p(d_2|H_0)$ becomes $p(d_2|H_0) = \int_\beta^\infty p(\ell|H_0)d\ell$ and $\beta = 2\ln\lambda + n(\log|\Sigma| + \mathrm{tr}\Sigma^{-1}S - |S|)$

5 RESULTS AND DISCUSSION

We can define by $Z_0 = \{\mathbf{z}|\ell(\mathbf{z}) < \beta\}$ and $Z_1 = \{\mathbf{z}|\ell(\mathbf{z}) \geq \beta\}$ two subsets of the n-dimensional space. Therefore the conditional probability that $\mathbf{z} \in Z_1$ (resp. Z_2) is just the conditional probability that $\ell(\mathbf{z})$ is less (resp. greater) than β, *i.e.* HVS burst vs only noise. Detected HVS patterns are shown in Fig. 5, with $\eta = 1$ (no prior).

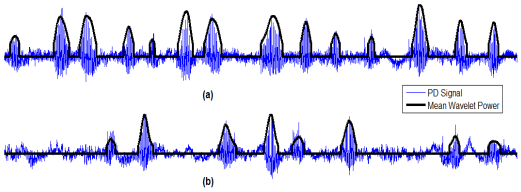

Figure 5: Illustration of the detection of PD of HVS burst.

Table 1: Main results number of burst detected with respect to signal on noise ratio (SNR).

# sensors	**Signal on noise ratio**		
3	7	21	20
5	12	24	41
6	21	29	65
8	39	50	88

For short, the performances, as expected, increase with the number of sensors and a high SNR.

6 CONCLUSION

The proposed plan enable us to detect most HVS episodes at its onset from the local field potentials recorded from awake, freely moving rats and to trigger the delivery of stimulations with arbitrary waveforms onto particular brain regions upon detecting HVSs automatically. More generally, it could help to improve the existing biometrics methods through better *event detection* and apparently it is well adapted for multidimensional signal. Previous results show that the proposed filter detects about 90% of the events and commits few errors, ensuring that most HVS episodes identified are in agreement with reality.

This corpus of methods relies on a running time window whose window length ($0.5-1$s) is too long to efficiently stop individual HVSs episodes ($1-4$ s). Under this concern we will investigate in the future the feasibility of using dynamical models to predict the occurrence of a HVS before its onset and study if β-waves can be induced by artificially evoked HVSs

REFERENCES

Clancy, E. and Farry, K. (2000). Adaptive whitening of the electromyogram to improve amplitude estimation. *IEEE Trans Biomed Eng.*, 47(6).

Cover, T. and Thomas, J. (1991). *Elements of Information Theory*. John Wiley and Sons.

DeFreitas, J., Beck, T., and Stock, M. (2012). Comparison of methods for removing electromagnetic noise from electromyographic signals. *Physiological Measurement*, 33(2):147.

Denzler, J. and Brown, C. (2002). Information theoretic sensor data selection for active object recognition and state estimation. *IEEE trans. on Pat. Anal. and Mach. Intel.*, 24(2):145–156.

Johnson, B. A., Abramovich, Y. I., and Scharf, L. L. (2011). Detectionestimation of multi-rank gaussian sources using expected likelihood. *Digital Signal Processing*, 21(5):568 – 575.

Miyano, H., Masuda, T., and Sadoyama, T. (1980). A note on the time constant in low-pass filtering of rectified surface emg. *IEEE Trans Biomed Eng.*, 27(5):274–8.

Perumal, R. and Chen, H. (2014). Performance analysis in a wavelet-based algorithm for automatic detection of high-voltage spindles in parkinson's disease rat models. In *9th Asian-Pacific Conference on Medical and Biological Engineering*, Tainan, Taiwan.

Radek, R. J., Curzon, P., and Decker, M. W. (1994). Characterization of high voltage spindles and spatial memory in young, mature and aged rats. *Brain Research Bulletin*, 33:183188.

Sitnikova, E., Hramov, A. E., Koronovsky, A. A., and van Luijtelaar, G. (2009). Sleep spindles and spike-wave discharges in eeg: their generic features, similarities and distinctions disclosed with fourier transform and continuous wavelet analysis. *J. Neurosci. Methods*, 180:304316.

Vigneron, V. and Jutten, C. (2004). *Independent Component Analysis and Blind Signal Separation*, volume LNCS 3195 of *Lectures Notes in Computer Science*, chapter Fisher Information in Source Separation Problems, pages 168–176. Springer.

Vigneron, V., Syed, T., Montagne, C., Barlovatz-Me imon, G., and Lelandais, S. (2010). Template matching and test detection. Application to cell l ocalization in cells imagery. *Pattern Recognition Letters*, 31(14):2214–2224.

Vrins, F., Jutten, C., and Verleysen, M. (2004). *Fifth International Conference, ICA 2004*, volume LNCS 3195, proceedings Sensor array and electrode selection for non invasive fetal electrocardiogram extraction by Independent Component Ananlysis. Springer-Verlag, Granada, Spain.

Yao, K., Hudson, R., D., C., and Lorenzelli, F. (1998). Blind beamforming on a randomly distributed sensor array system. *IEEE Journal on selected areas in communication*, 16(8):1555–1566.